Arabian Journal of Chemistry (2023) **16**, 104666

King Saud University

Arabian Journal of Chemistry

www.ksu.edu.sa
www.sciencedirect.com

ORIGINAL ARTICLE

Selective liquid-phase oxidation of toluene over heterogeneous Mn@ZIF-8 derived catalyst with molecular oxygen in the solvent-free conditions

Shaobin Deng [a], Gui Chen [a,b,*], Chunhua Liang [c], Linjie Wang [a], Bailin Xiang [a,*]

[a] *College of Chemistry and Materials Engineering, Huaihua University, Huaihua 418000, PR China*
[b] *School of Chemical Engineering, Xiangtan University, Xiangtan 411105, PR China*
[c] *School of Life and Health Science, Kaili University, Kaili 556011, PR China*

Received 8 November 2022; accepted 8 February 2023
Available online 15 February 2023

KEYWORDS

Molecular oxygen;
Mn@ZIF-8;
Toluene;
Benzaldehyde;
Benzyl alcohol

Abstract In this work, liquid-phase catalytic oxidation of toluene was carried out under solvent-free conditions, and highly selective synthesis of benzaldehyde (BAL) and benzyl alcohol (BOL) and benzoic acid (BAC) in the presence of Mn@ZIF-8 calcined material as catalyst with oxygen molecules. As a heterogeneous catalyst, the zeolitic imidazolate framework Mn@ZIF-8 derived material exhibited reasonable substrate-product selectivity (70.3% of selectivity to BAL and BOL, 95.1 % of selectivity to BAL, BOL and BAC) and conversion (6.5%) under optimum reaction conditions. The catalysts were characterized by BET-specific surface area determination, XRD, XPS, FT-IR, TG-DTG and SEM-EDS-Mapping. The results demonstrated that the catalytic capacity of the catalysts was enhanced by the good dispersion of amorphous Mn species in ZIF-8 derivatives and high specific surface area. The possible reaction pathway for the catalytic oxidation of toluene was also suggested. Maybe this method employing Mn@ZIF-8 as efficient catalyst affords a new and environmentally friendly route for the synthesis of BOL and BAL from the selective oxidation of toluene.

1. Introduction

As every-one knows, liquid-phase oxidation of toluene has been critical to the development and utilization of fine chemicals (aromatic alcohol and aldehydes) from organic chemical material (Gardner and Mayer, 1995; Tan et al., 2017). The partial oxidation of toluene is an important method for the preparation of benzaldehyde (BAL), benzyl alcohol (BOL) and benzoic acid (BAC) (Somma et al., 2017; Chen et al., 2022). BOL and BAL are important chemical intermediates with high added value, it is widely used in industrial chemical production as organic synthesis raw materials, solvent, stabilizer and preservation, daily chemical essence, and so on (Alabbad et al., 2014; Assal et al.,

* Corresponding authors at: College of Chemistry and Materials Engineering, Huaihua University, Huaihua 418000, PR China.
E-mail addresses: cg@hhtc.edu.cn (G. Chen), xbl@hhtc.edu.cn (B. Xiang).

Peer review under responsibility of King Saud University.

Production and hosting by Elsevier

https://doi.org/10.1016/j.arabjc.2023.104666
1878-5352

2019; Rezaei et al., 2017; Zhang et al., 2011). In addition, BAC is an important bulk raw materials for the preparation of sodium benzoate preservatives, and the additives for drugs, dyes (Afnan et al., 2020; Zhu et al., 2016). The methods of toluene as the raw material to prepare BAL and BOL, such as benzyl chloride hydrolysis, indirect electrooxidation, and gas-phase partial oxidation, are extensive limited; mostly because the product obtained by these methods contains chlorine, high environmental pollution and excessive power consumption (Ding et al., 1996; Brown and Hudson, 1951). Due to advantages of environment-friendly way, high atom utilization and suitable reaction conditions, liquid-phase oxidation of toluene is an important method for the preparation of oxygen-containing compounds (Scheme 1). In the oxidation of toluene, heterogeneous catalyst has widespread application, due to their remarkable advantages in efficient selectivity of products, catalyst recovery and utilization, post-processing.

However, in the early research process of catalytic oxidation of toluene used peroxide as oxidant, acetic acid as solvent, bromide salt as assistant. Now, it mostly used expensive catalyst in the case of no assistant solvent, such as metal porphyrin, doped Pd, Au and other precious metals catalysts, or that catalyst with complex preparation process. For instance, Wang et al. (Wang et al., 2009) explored bis (acetylacetonato) oxovanadium ($VO(acac)_2$) catalysts for toluene oxidation with H_2O_2 as oxidant in acetic acid, giving 19.8 % conversion of toluene and 56.1 % selectivity to BAL + BOL, 22.2 % selectivity to BAC. Hu et al. (Hu et al., 2006) investigated metalloporphyrin catalyst μ-oxo-bis[tetra-phenylporphyrin (III)] to catalyze toluene oxidation, the conversion was 7.4 %, the selectivity to BAL + BOL was 59.0 %. In another study, Zhang et al. (Zhang et al., 2008) immobilized Au-Pd alloy nanoparticles on carbon or TiO_2 as catalysts to oxidize toluene under solvent-free conditions, the main products are benzyl benzoate (greater than 80 % selectivity) and the by-products are BAL and BAC. Jiang et al. (Jiang et al., 2013) used Au-γMnO_2 catalysts for solvent-free toluene oxidation with oxygen, giving 13.5 % conversion of toluene and 67.6 % selectivity to BAL + BOL, 16.8 % selectivity to BAC, 15.6 % selectivity to benzyl benzoate. Therefore, the development of efficient catalysts that are high toluene conversion and efficient selectivity to BAL, BOL in an O_2-based system is a great challenge.

Recently, metal–organic frameworks (MOFs) were received considerable attention to catalytic reaction, oxidative degradation and electrochemical sensing because of their properties, such as large surface area, well-defined structures, structural diversity and easy processing (Taghavi et al., 2022; Dehdashtian et al., 2022; Alamgholiloo et al., 2020; Alamgholiloo et al., 2021; Zhao et al., 2020). Pliekhov et al. (Pliekhov et al., 2018) reported Co-MOF-74@NDHPI catalytic system with 16 % toluene conversion; and good selectivity to BAL + BOL (66.0 %) and relatively higher selectivity to BAC (34.0 %), resectively. However, their application is limited by their complicated preparation process and expensive raw materials (Jiang et al., 2010). To our delight, this research has led to a strong interest in catalytic oxidation of toluene using MOFs or zeolitic imidazolate frameworks (ZIFs) to find low-cost, simple and efficient mono-metal-doped metal–organic frameworks catalytic system (Hu et al., 2018; Mohtasham et al., 2022).

Carry on with our work, we successfully synthesized Mn@ZIF-8. Furthermore, based on the previous researcher of liquid-phase oxidation reactions in the solvent- and additives-free conditions (Ni et al., 2021; Jian et al., 2020; Liu et al., 2019; Chen et al., 2022); we will report a simple eco-friendly method for synthesis of BAL, BOL employing Mn@ZIF-8 derived material as an effectual catalytic system for the partial oxidation of toluene with oxygen in this work. This is the meaningful report about the oxidation of toluene to three oxidation products in industry.

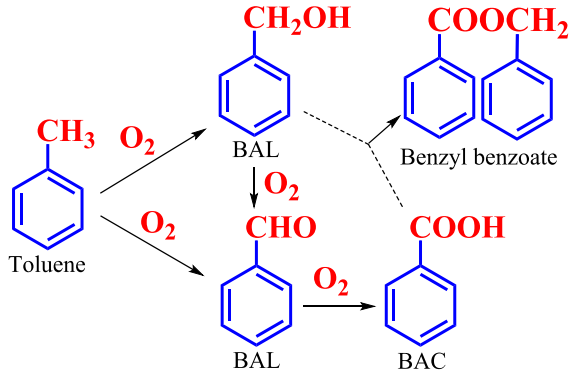

Scheme 1 Routes of the synthesis of BOL, BAL and BAC.

2. Experimental

2.1. Reagents and instrument

$Mn(CH_3COO)_2{\cdot}4H_2O$ (AR, 99.0 %) was obtained from Tianjin Guangfu Fine Chemical Institute, China. Toluene (AR, 99.5 %), $Zn(NO_3)_2{\cdot}6H_2O$ (AR, 99.0 %) and $Ce(NO_3)_3{\cdot}6H_2O$ (AR, 99.0 %) were gained from Sinopharm Chemical Reagent Co., ltd., China. 2-Methylimidazole (AR, 99.0 %) and other reagents were purchased from Shanghai Mclean Co., ltd. Miniature high pressure reactor (BE100) was obtained from Shanghai LABE Instrument Co., ltd. GC–MS qualitative analysis of all products was carried out by Japan Shimadzu GCMS-QP2010 plus. The quantitative analysis of reaction products was detected by GC Agilent 7890B with HP-5 column and hydrogen flame ion detector.

2.2. Catalyst preparation

Mn@ZIF-8 was synthesized by solvothermal method (Zheng et al., 2020). Typically, Mn@ZIF-8 with the 10:1 Zn/Mn molar ratio was prepared by the following steps: firstly, 0.2 g $Mn(CH_3COO)_2{\cdot}4H_2O$, 0.6 g 2-methylimidazole and 2.1 g Zn $(NO_3)_2{\cdot}6H_2O$ were added into 126.5 mL *N*,*N*-dimethylformamide under stirring, and then set in a 200 mL autoclave. After autoclaving at 140 °C overnight, the resulting powder was rinsed repeatedly with anhydrous ethanol, dried at low temperature, then calcined at 300 °C for 2.0 h under air atmosphere (static in muffle) to acquire the fresh Mn@ZIF-8 derived catalyst, and the catalyst after reuse was calcined and defined as regenerated catalyst. Other MOF series catalysts (MOF-5, MOF-74) were prepared according to reference (Pliekhov et al., 2018; Xiang et al., 2019).

2.3. Catalyst characterization

The nitrogen adsorption–desorption isotherms were collected by a Quantachrome NOVA-2200e (Degassing was performed at high vacuum for 12 h, followed by N_2 adsorption tests at 77 K). XRD analysis were tested by a Rigaku D/Max-2550 V^+ diffractometer (Single source CuKα target diffraction source, λ = 1.5418 Å, working voltage 30 kV, working current 40 mA, 2θ = 5-90°, scanning speed 10°/min). XPS analysis were recorded by a ESCALAB 250Xi analyser (Al Ka (1486.6e V) with monochromator as the X-ray excitation source, 150 W power, C 1 s, 284.8 eV). FT-IR spectra were measured on a Nicolet-380 instrument in the range of 4000–400 cm^{-1} (High purity KBr tablets were pressed and then tested). TG/DTG curves were tested by a Mettler thermogravi-

metric analyser (Vacuum dried at 105 °C for 12 h, the air flow rate was 40 mL/min, and the room temperature was heated to 800 °C at a rate of 10 °C/min). SEM images were obtained with Sigma HD, Carl Zeiss (FE-SEM, 20 kV acceleration voltage).

2.4. Catalytic experimental procedure

Typically, 21.0 g toluene and 0.1 g Mn@ZIF-8 derived catalyst were added into the 100 mL stainless steel reactor. When the temperature of reactor heated to a certain temperature, molecular oxygen in a high-pressure oxygen tank was continuously put into the reaction equipment after decompression. The reaction was implemented at 180 °C and 1.0 MPa for 2.5 h with 800 r/min stirring. After reaction, the resulted products were quantified by GC (the internal standard substance chlorobenzene).

The toluene conversion and the selectivity to BOL, BAL and BAC were calculated using the following formulas.

$$\text{Conversion of toluene} = \frac{\text{the mole of toluene reacted}}{\text{the mole of toluene added}} \times 100\% \quad (1)$$

$$\text{Selectivity of BOL}\,(\%) = \frac{\text{the mole of BOL}}{\text{the mole of toluene reacted}} \times 100\% \quad (2)$$

$$\text{Selectivity of BAL}\,(\%) = \frac{\text{the mole of BAL}}{\text{the mole of toluene reacted}} \times 100\% \quad (3)$$

$$\text{Selectivity of BAC}\,(\%) = \frac{\text{the mole of BAC}}{\text{the mole of toluene reacted}} \times 100\% \quad (4)$$

3. Results and discussion

3.1. Catalyst characterization

3.1.1. Textural analysis and X-ray diffraction (XRD)

BET-specific surface area determination of fresh and regenerative samples are shown in Fig. 1. The isotherms of two samples have a type-IV curve (type-H3 hysteresis loop), exhibiting the presence of abundant mesoporous structures (Lü et al., 2020; Movahed et al., 2018). Meanwhile, Table 1 shows the textural properties of regenerative sample have little change compare with fresh sample, attributing to great number of C species of the catalyst in the calcination process. ICP result shows low levels of Mn in the catalyst. In addition, two samples have large specific surface area (greater than650 m^2/g), which is one of the reasons for their good catalytic performance. This is consistent with the experimental results.

Fig. 2 exhibits the XRD curves of four samples. Firstly, the pattern of ZIF-8 was consistent with that reported previously (Abdollahi et al., 2021), confirming the formation of pure crystalline ZIF-8 phase (Jing et al., 2014).The four diffraction peaks appear at 31.8°, 34.4°, 36.3° and 47.5°, belonging to ZnO (JCPDS 36–1451). Compared with ZnO, the patterns of ZIF-8 and Mn@ZIF-8 show specific diffraction peaks. As expected, the characteristic peak (1 1 0) of ZIF-8 at 7.3° was found in four samples. However, the introduction of manganese species in this catalyst leaded to its weakening at 7.3°.

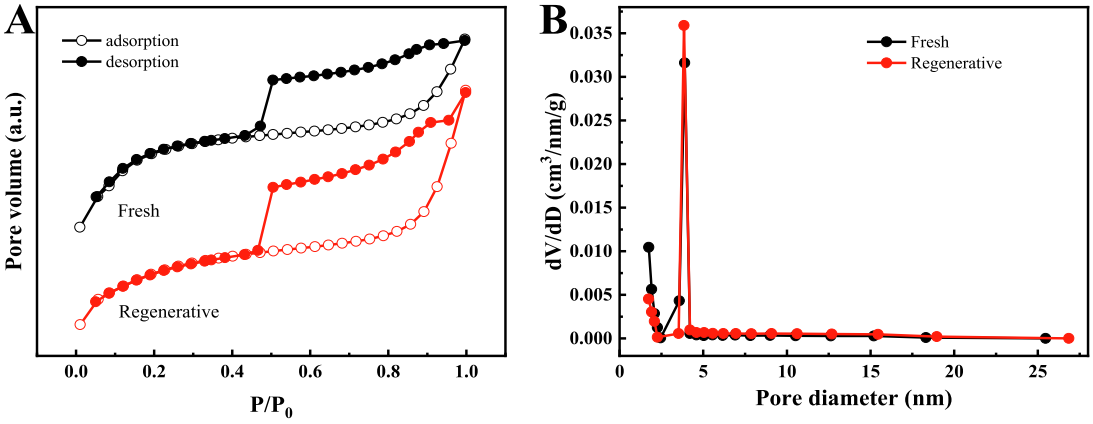

Fig. 1 N_2 adsorption–desorption isotherms(A) and pore diameter distribution curves of samples(B).

Table 1 Textural properties of samples.

Samples	ICP (m_{Zn}/m_{Mn})	Surface area (m^2/g)	*t*-plot micropore area (m^2/g)	Pore volume (cm^3/g)	*t*-plot micropore volume (cm^3/g)	Pore diameter (nm)
Fresh	161/1	669.7	394.9	0.44	0.21	2.62
Regenerative	157/1	654.5	348.4	0.42	0.19	3.05

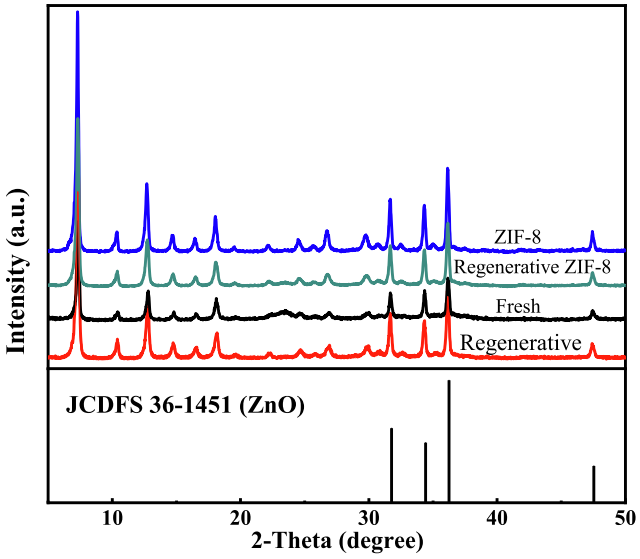

Fig. 2 XRD curves of samples.

Even more, XRD pattern of Mn@ZIF-8 didn't have a diffraction peak assigned to Mn species, indicating that the Mn species may be present in the framework of the molecule, or the Mn content was below the detection limit (Liu et al., 2016; Deng et al., 2017).

The average crystallite sizes of four samples are calculated with the Scherrer equation (Ho et al., 2020), the crystallite size of fresh, regenerative samples, ZIF-8 and regenerative ZIF-8 were 38.5, 43.0, 55.5 and 59.2 nm, respectively. It indicated that manganese was successfully incorporated into the catalyst, resulting in a smaller grain size. Combined with the experimental results, its catalytic performance was enhanced.

3.1.2. X-ray photoelectron spectroscopy (XPS)

XPS measurement was conducted to probe the electrons of C 1 s, N 1 s, O 1 s, Mn 2p3/2 and Zn 2p centered at 284.8, 398.9, 531.4, 641.5 and 1021.7 eV, respectively (Fig. 3A). Fig. 3B displays C 1 s spectra, it is fitted into three peaks centered at 284.8 eV (C—C), 286.3 (C—N), and 288.1 (*N*-C=N), respectively (Zhao et al., 2020). However, due to the effects of oxidation reaction, the *N*-C=N is a little bit of a shift towards

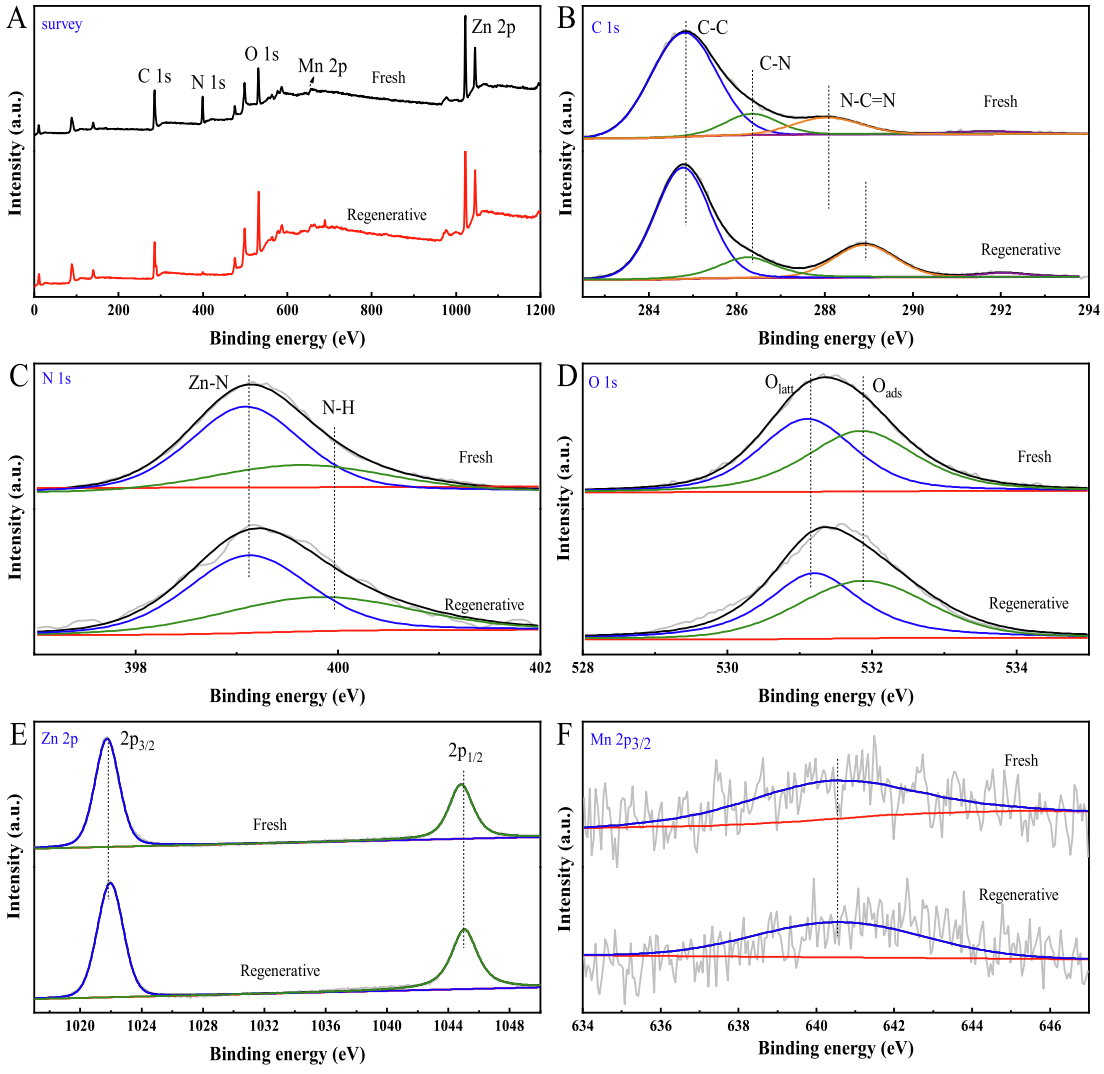

Fig. 3 XPS spectra of samples.

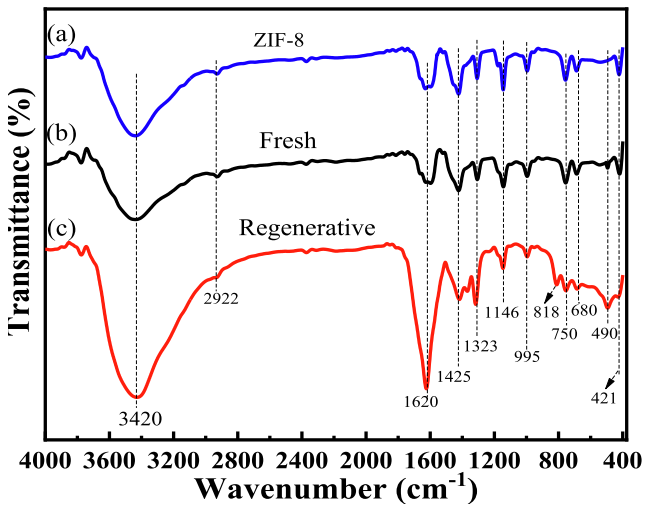

Fig. 4 FT-IR spectra of samples.

higher electron volts (An et al., 2022). Fig. 3C shows the N 1 s spectra, it can be fitted into two peaks at 399.9 eV (N—H) and 398.8 eV (Zn-N), this is in good agreement with previously reported (Ran et al., 2020). The O 1 s spectra are decomposed into two peaks containing different oxygen chemical bonds (Fig. 3D). The first peak at the lower bond energies (531.1 eV) is attributed to lattice oxygen (Olatt). Another peak (531.8 eV) is ascribed to chemisorption oxygen or weakly bonded oxygen (Oads) (Du et al., 2018). Fig. 3E shows the Zn 2p spectra of the catalysts, which are decomposed into two peaks (1044.9 and 1021.8 eV) (Zhao et al., 2020; Ran et al., 2020; Li et al., 2022). The Mn 2p3/2 peak (640.5 eV) correspond to superficial Mn^{2+} species (Fig. 3F), the chemical state of the superficial Mn species on the catalysts is Mn^{2+} (Musić et al., 2009). Combined XRD analysis, it indicated that the Mn species may be present in the framework of the molecule.

3.1.3. Fourier transform infrared spectrogra (FT-IR) and thermal stability characterization

FT-IR (Fig. 4) exhibits many characteristic peaks of three samples. A sharp peak (421 cm^{-1}) is attributed to a typical Zn-N stretching vibration, it indicates that Zn-N form a porous ZIF-8 coordination structure (Jing et al., 2014; Nagarjun and Dhakshinamoorthy, 2019). The peaks at 680 (C—H bending), 750 (C—H bending), 1323 (CH_2 wagging) and 2922 cm^{-1} (C—H symmetric stretch) correspond to the bending signals of the imidazole ring (Movahed et al., 2018; Yang et al.,

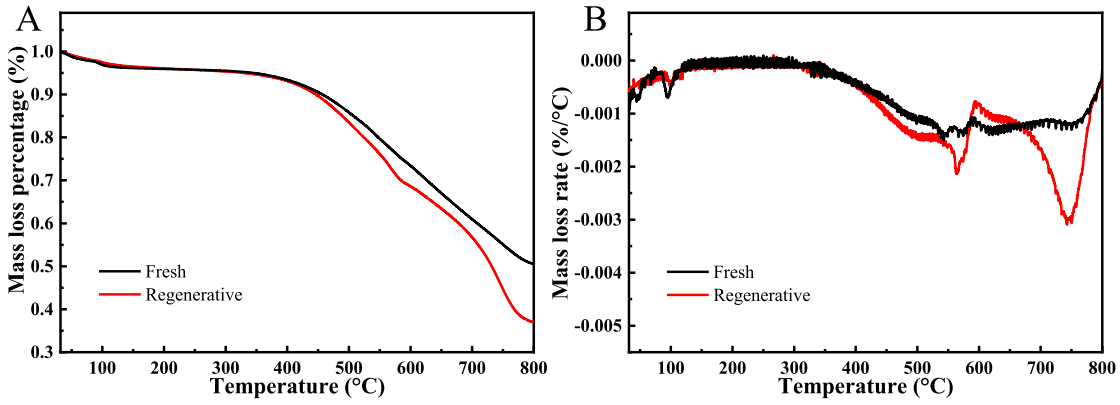

Fig. 5 TG (A) and DTG (B) curves of samples.

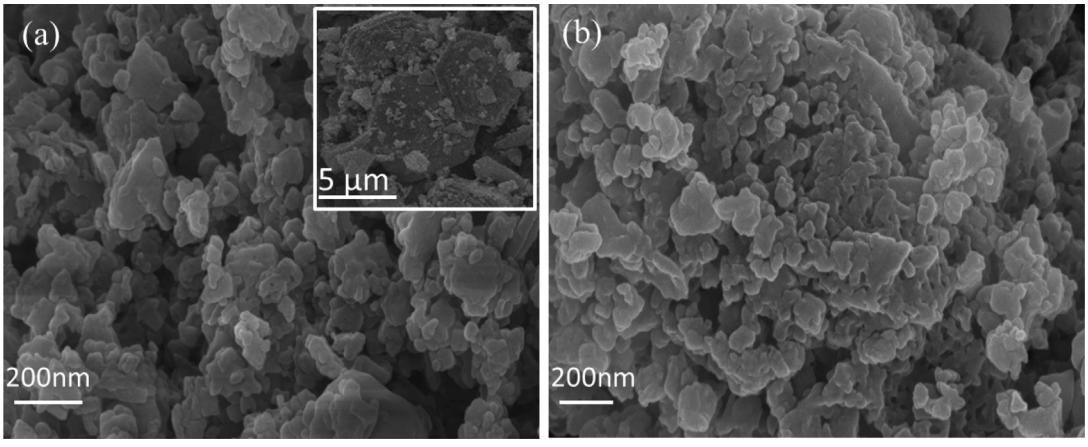

Fig. 6 SEM images of fresh(a) and regenerative (b) samples.

2018; Mohammed et al., 2021). Furthermore, the peaks at 995 (=C—H in-plane bend), 1146 (=C—H in-plane deformation vibration), 1425 cm^{-1} (CH_2 asymmetric bend) are the stretching vibration of the imidazole ring (Zhao et al., 2020; Yang et al., 2018). At 490 cm^{-1} for fresh and regenerative samples, it can be ascribed to Mn-O stretching vibration (Musić et al., 2009; Wang et al., 2020). The broad peak (3420 cm^{-1}) was assigned to –OH deformation vibration and N—H stretching mode (Zhang et al., 2020). The peak (1620 cm^{-1}) can be ascribed to C=N stretch/ C=C stretching vibration (Asadzadeh-Khaneghah et al., 2021; Awadallah-F et al., 2019; Chen et al., 2019). However, compared with ZIF-8, fresh and regenerative samples have two new peaks at 1375 (CH_3 asymmetric bend) and 818 cm^{-1}, which may be caused by the product left over from the reaction process. The results demonstrated that the chemical structure of the Mn@ZIF-8 derived samples did not change significantly after regeneration, so that its catalytic performance had a little change in the oxidation of toluene.

Fig. 5 shows the TG/DTG curves of two samples. Main weight loss of two samples are concentrated between 350 and 800 °C, meaning to the collapse of the frameworks of ZIF-8 (Fu and Ren, 2020). Notably, the regenerative catalyst exhibits a higher percentage of weight loss, implying that organic matters of the toluene reaction process are primarily embedded in the interior of the Mn@ZIF-8 derived catalyst. These results showed that the catalyst had good thermo-stability in the oxidation of toluene (reaction temperature is lower than 200 °C) (Yang et al., 2018; Wen et al., 2021; Abdelmigeed et al., 2021).

3.1.4. Morphology and element distribution characterization

SEM characterization is shown in Fig. 6. The shape of samples exhibits polyhedron morphology with size of 6 μm (Guo et al., 2018). Fresh sample is small and irregular pieces (Son et al.,

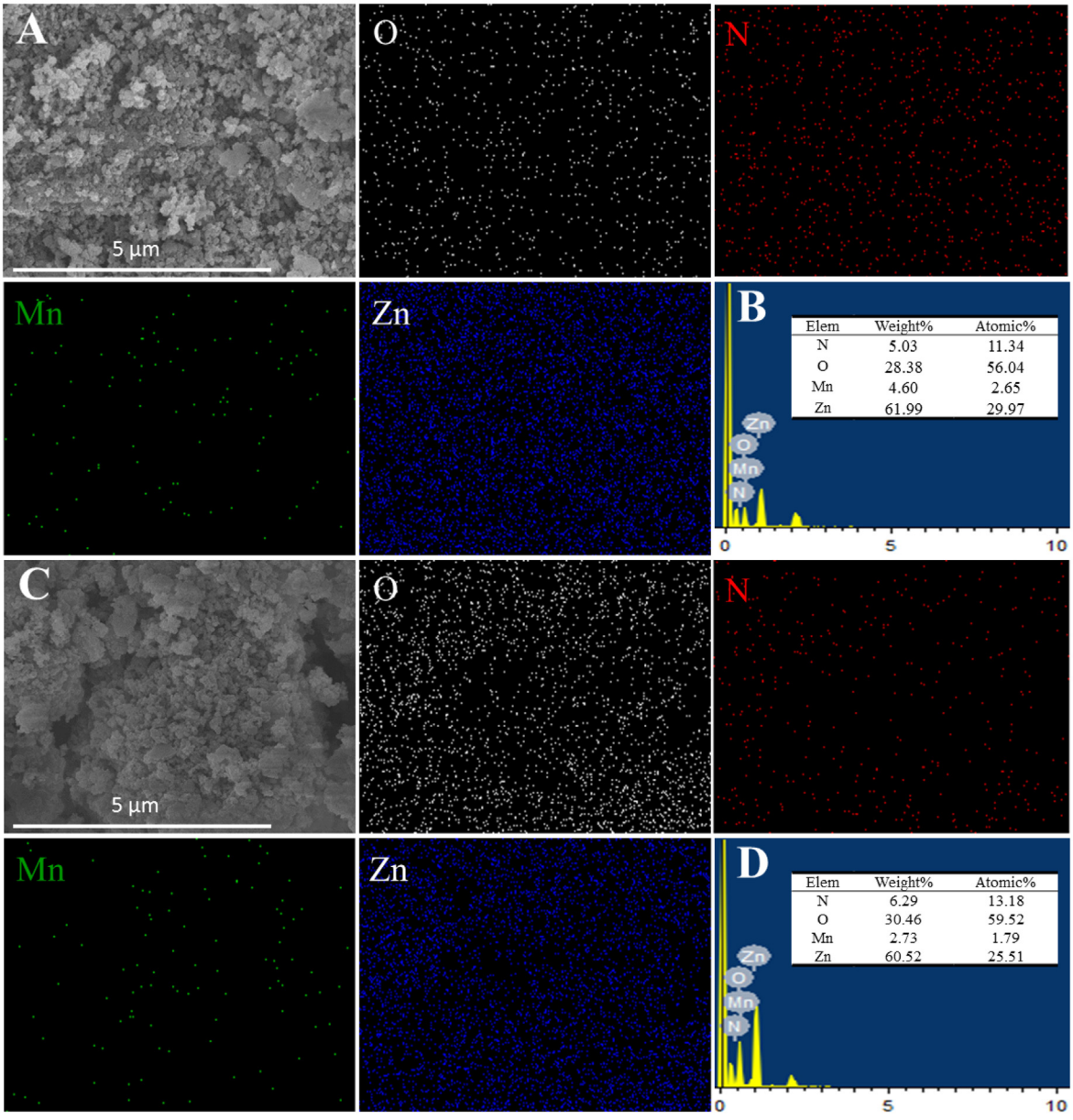

Fig. 7 SEM-Mapping images and EDS analyzer of fresh (A, B) and regenerative samples (C, D).

2019). However, regenerative sample is a little aggregated particle. In the process of toluene oxidation reaction, combined with repeated experiments, carbon deposition had a little impact on the morphology and catalytic activity of the catalyst.

The elemental mappings and EDS were done to identify the presence and distribution of four elements (O, N, Mn and Zn) in the two samples (Fig. 7). It indicates that O, N, Mn and Zn are distributed relatively uniformly within two samples. It is noteworthy to mention that the homogeneity of four elements is one reason for its excellent performance in the reaction process (Hao et al., 2018). However, the element ratio of the regenerative sample is different with the fresh sample, which may be the reason for a little decrease of catalytic activity.

3.2. Catalytic performance

To find an effective catalyst, we examined some MOFs catalysts in the oxidation of toluene (Table 2). Actually, BAL and BOL were obtained in the oxidation of toluene without any catalysts, only 2.5 % of toluene conversion (**entry 1**). To our delight, it was showed good catalytic activity of ZIF-8 with 5.1 % toluene conversion, 73.6 % selectivity to BAL + BOL (**entry 2**). However, other catalysts were weak catalysts (**entries 3–6**).

Next, we attempted to incorporate Mn during the in-situ synthesis catalyst to enhance the catalytic activity of MOFs (**entries 7–9**). Compared with other catalysts, the addition of Mn into ZIF-8 ungently improve the catalytic activity. These results indicates that Mn and ZIF-8 of this catalyst have an interaction and improve the oxidation activity.

3.3. Effect of the preparation factors of catalyst

The performance of Mn@ZIF-8 derived catalyst with the different molar ratio of Zn/Mn and calcination temperature were also explored. As shown in Table 3 and Table 4, With the decrease of Zn/Mn molar ratio, the toluene conversion

Table 2 Catalytic performance comparison of catalysts.[a]

Entry	Catalyst	Conversion (%)	Selectivity (%)					
			BAL	BOL	BAC	BAL + BOL	Total [b]	Others [c]
1	None	2.5	41.2	30.8	23.7	72.0	95.7	4.3
2	ZIF-8	5.1	38.0	35.5	22.0	73.5	95.5	4.5
3	MOF-74	2.6	56.4	27.4	13.1	83.8	96.9	3.1
4	MOF-5	2.9	55.4	22.0	21.9	77.4	99.3	0.7
5	ZnO	3.9	40.4	31.9	23.3	72.3	95.6	4.4
6	MnO	4.2	44.6	30.2	19.0	74.8	93.8	6.2
7	Mn@MOF-74	5.8	34.5	33.6	26.6	68.1	94.7	5.3
8	Mn@MOF-5	7.0	27.2	21.2	47.8	48.4	96.2	3.8
9	Mn@ZIF-8	6.5	31.6	38.7	24.8	70.3	95.1	4.9

[a] Reaction conditions: toluene 21.0 g, reaction temperature 180 °C, 0.1 g catalyst, oxygen pressure 1.0 MPa, reaction time 2.5 h, Zn/Mn molar ratio 10:1.
[b] The selectivity of three main oxidation products.
[c] By-products were methylbiphenyl, benzoquinone, and benzyl benzoate.

Table 3 Effects of Zn and Mn molar ratio.[a]

Zn/Mn (molar ratio)	Conversion (%)	Selectivity (%)					
		BAL	BOL	BAC	BAL + BOL	Total	Others
20/1	5.5	33.2	37.2	24.9	70.4	95.3	4.7
10/1	6.5	31.6	38.7	24.8	70.3	95.1	4.9
5/1	6.9	25.6	30.1	37.1	55.7	92.8	7.3

[a] Reaction conditions: 300 °C calcination temperature, 21.0 g toluene, 0.1 g Mn@ZIF-8, 180 °C, 2.5 h, 1.0 MPa.

Table 4 Effects of calcination temperature.[a]

Calcination temperature (°C)	Conversion (%)	Selectivity (%)					
		BAL	BOL	BAC	BAL + BOL	Total	Others
300	6.5	31.6	38.7	24.8	70.3	95.1	4.9
500	3.4	46.0	35.5	13.8	81.5	95.3	4.7
700	3.4	46.0	34.4	15.4	80.4	95.8	4.2
900	3.2	39.9	35.9	19.7	75.8	95.5	4.5

[a] Reaction conditions: 0.1 g Mn@ZIF-8, 21.0 g toluene, 180 °C, 2.5 h, 1.0 MPa.

revealed an upward trend. As the calcination temperature is too high, ZIF-8 skeleton is collapses, which leads to the degradation of catalytic performance (Li et al., 2006; Zhang et al., 2018). when Zn/Mn molar ratio and calcination temperature were 10:1 and 300 °C, respectively, BOL + BAL were obtained the highest selectivity (70.3 %) under the same conditions.

3.4. Reaction conditions optimization

This work optimized the toluene oxidation reaction parameters (in Fig. 8). Fig. 8A and 8B showed that the conversion of toluene was gently increased, while BOL + BAL selectivity displayed trend downward with raised the amount of catalyst and oxygen pressure, and the BAC selectivity was increased, other by-products were both increased gradually in a small range. It was that aromatic alcohols and aldehydes could be increase acceleratory oxidized to other productes in higher reaction parameters.

However, with the increase of reaction time and reaction temperature (Fig. 8C and 8D), the conversion of toluene was an increasing trend firstly, and then decreasing trend, BOL + BAL selectivity showed a falling trend firstly, and then increasing trend, while the selectivity to other by-products were opposite to the trend of BOL + BAL. For reaction time, the performance of catalyst could not be fully exerted when reaction was in the induction phase (Fan et al., 2017) (1.5 h), so the BOL + BAL selectivity was very high. Finally, the pressure of the gas phase toluene also increased as the temperature rising gradually, and the molecular oxygen was actually decreases in the reactor, so it was leaded to the above results (Fu et al., 2022).

Therefore, under the oxidation of toluene reaction conditions: 21.0 g toluene, 180 °C, reaction time of 2.5 h, 0.1 g Mn@ZIF-8 derived catalyst, oxygen pressure of 1.0 MPa, a good substrate-product selectivity (70.3 % of BOL + BAL, 95.1 % of total selectivity to three products) and conversion (6.5 %) were obtained.

3.5. The recycle of Mn@ZIF-8 derived catalyst in the toluene oxidation

The recycle of heterogeneous Mn@ZIF-8 derived catalyst was used in the reaction under the above optimal conditions. Firstly, the catalyst separated by the centrifugation after reaction, washed with ethanol, dried at 105 °C. After calcining at 300 °C for 2.0 h, it was used the following reaction.

As shown in Fig. 9, it was clear that the catalytic activity of recovered catalyst was stable in five runs, the selectivity to BAL + BOL maintained 69.4 % with 5.8 % of toluene conversion. The results indicated that the stability and catalytic activity of Mn@ZIF-8 was a litter changed in the recycle oxidation reaction.

3.6. Performance comparison of catalysts reported in the literatures

Table 5 shows the catalytic results of different catalysts in the literatures. It can be seen that different catalytic systems require different reaction conditions, and the toluene conver-

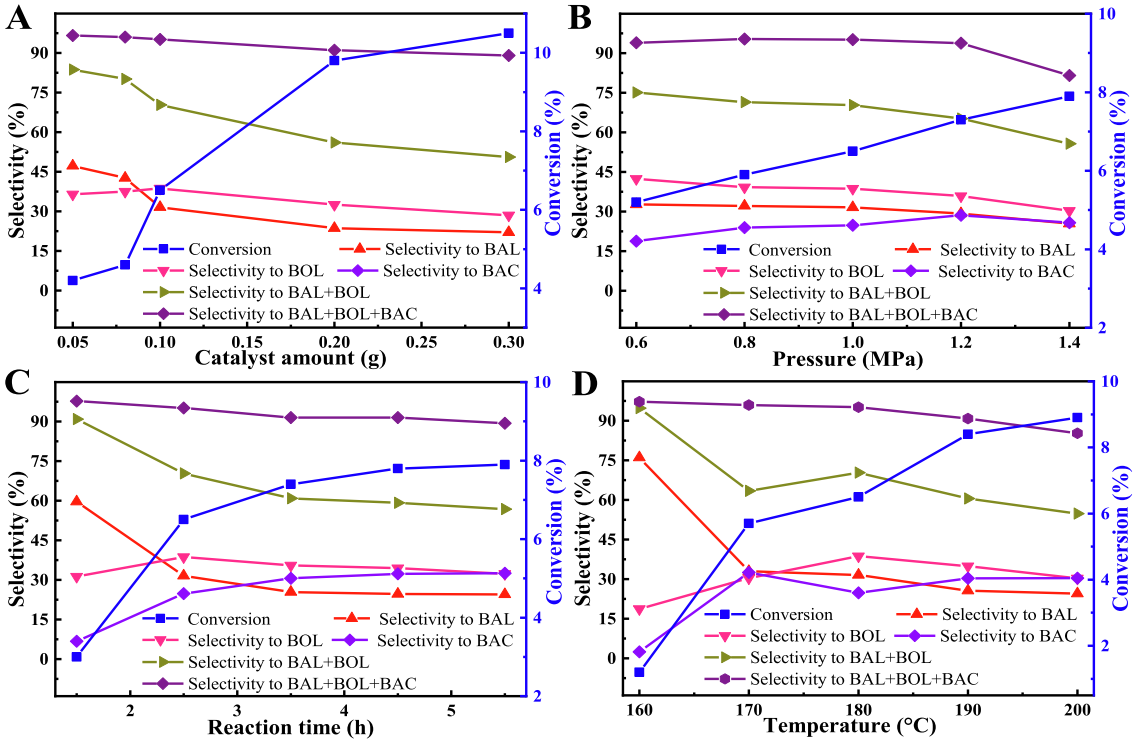

Fig. 8 Optimization of reaction parameters. Influences factors: (A) 1.0 MPa oxygen pressure, 180 °C reaction temperature, 2.5 h reaction time; (B) 0.1 g catalyst, 180 °C reaction temperature, 2.5 h reaction time; (C) 0.1 g catalyst, 1.0 MPa oxygen pressure, 180 °C reaction temperature; (D) 0.1 g catalyst, 1.0 MPa oxygen pressure, 2.5 h reaction time.

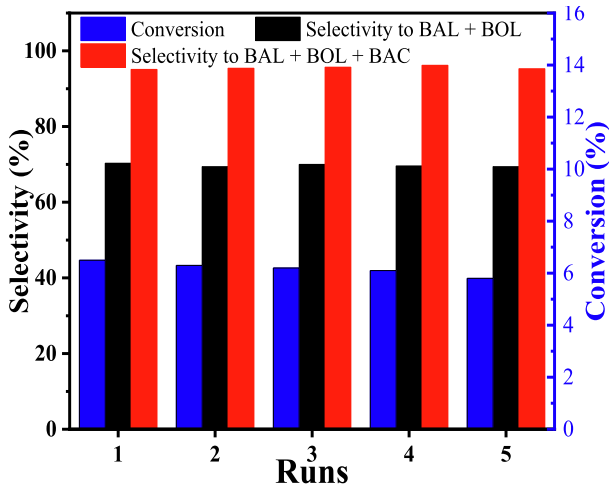

Fig. 9 Results of recycle of Mn@ZIF8 catalyst. Reaction conditions: 0.1 g Mn@ZIF-8, 1.0 MPa, 180 °C, 2.5 h, 21.0 g toluene.

sion is higher in the presence of solvents or additives, but these bring inconvenience to industrial production. If hydrogen peroxide is used as an oxidant, there are also safety problems in industry. Although noble metals or metalloporphyrins have high catalytic activity, their preparation process is complex and their stability is poor, which limits their industrial application. We reported a simple eco-friendly method for synthesis of BAL, BOL employing Mn@ZIF-8 as an effectual catalytic system for the partial oxidation of toluene with oxygen in this work.

3.7. Possible catalytic oxidation reaction pathway of toluene over Mn@ZIF-8 derived catalysts

Fig. 10 shows a possible catalytic oxidation reaction pathway of toluene to BAL and BOL over heterogeneous Mn@ZIF-8 derived catalyst. The catalyst has been critical effect at the beginning of the oxidation reaction through the activation of reactant toluene, and then formation of the benzyl radical (C_7H_7•) and the intermediate benzyl peroxyradical (ArOO•)

Table 5 The performance comparison of catalysts reported in the literatures.

Catalyst	Oxidizer	Solvent/ (Initiator)	Temperature (°C)	Time (h)	Conversion (%)	Selectivity (%)			Ref.
						BAL	BOL	BAC	
$VO(acac)_2$	H_2O_2	Glacial acid	90	4.0	19.8	50	6.1	22.2	(Wang et al., 2009)
Co-MOF-74@NDHPI	O_2	(NDHPI)	100	2.0	16.0	18.0	48.0	34.0	(Alamgholiloo et al., 2020)
Mn_3O_4/CNTs	O_2	(TBHP)	90	12.0	24.63	43.5	47.0	-	(Feng and Zeng, 2020)
Au-γMnO_2	O_2	–	160	8.0	13.5	3.5	64.1	16.8	(Jiang et al., 2013)
Pt/ZrO_2	O_2	–	90	3.0	37.2	19.6	6.5	70.4	(Ilyas and Sadiq, 2009)
$[TPPFe^{III}]_2O$	O_2	–	165	3.8	7.4	59.0		-	(Hu et al., 2006)
Co(II)TPP	air	–	160	3.5	8.9	33.0	27.0	39.0	(Guo et al., 2005)
Cu-Mn oxides	O_2	–	190	2.0	17.2	11.7	18.7	63.1	(Li et al., 2006)
NHPI/Cu-BTC	O_2	–	110	2.0	7.6	44.1	11.0	44.9	(Bao et al., 2016)
SO_4^{2-}/TiO_2-CeO_2	O_3-O_2	–	30	3.0	9.7	77.0			(Wang et al., 2009)
mpg-C_3N_4	O_2	–	160	16.0	3.1	99.0			(Li et al., 2012)
Mn@ZIF-8	O_2	–	180	2.5	6.5	31.6	38.7	24.8	[this work]

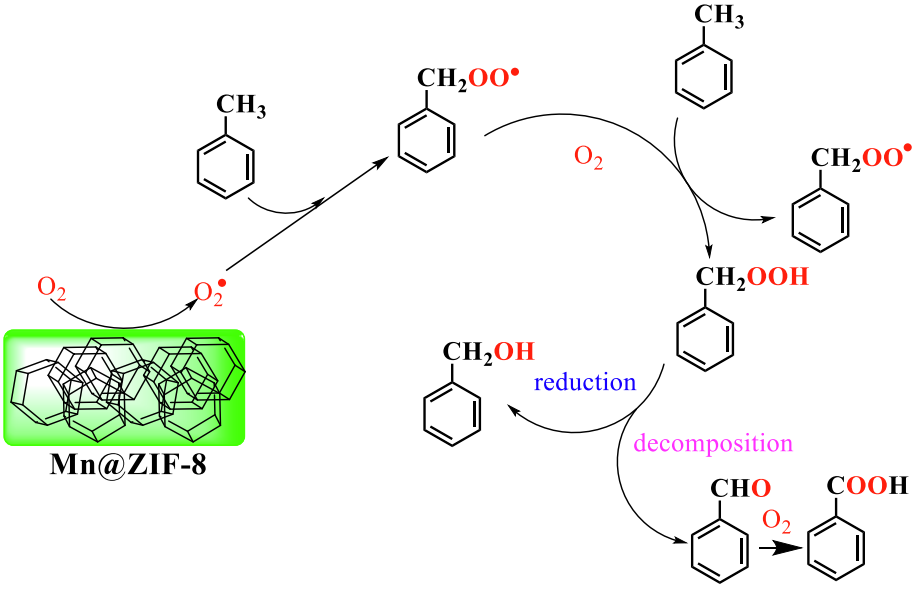

Fig. 10 Possible reaction pathway of toluene oxidation to BAL and BOL.

(Partenheimer, 2003). The reactive oxygen species can react with absorbed toluene to form the radical intermediate (ArOOH) (Biswas et al., 2020; Laribi et al., 2016). To prove the existence of the radical, *tert*-butylalcohol (hydroxyl radical scavenger) was add to the reaction system (Biswas et al., 2020). Just as we expected, a significant decrease of toluene conversion (1.2 %) was observed, which confirmed that the reactive radical intermediates reacted with *tert*-butylalcohol, resulting in a relative decrease of the toluene conversion. Finally, the resulting ArOOH intermediate were decomposed to BAL, and some of them were simultaneously reduced to BOL. The resulting BOL can be to BAL, even to BAC (Xu et al., 2021).

4. Conclusions

In summary, a novel Mn@ZIF-8 derived catalyst with low-cost, high catalytic activity, good heat resistance and stability was constructed, and used for the selective partial oxidation of toluene to BOL, BAL and BOL. 70.3 % selectivity to BAL + BOL with 6.5 % toluene conversion was acquired under optimum reaction conditions (21.0 g toluene, 180 °C, reaction time of 2.5 h, 0.1 g Mn@ZIF-8 catalyst, oxygen pressure of 1.0 MPa). Besides, the possible reaction pathway was suggested, and the results of characterization showed that the catalytic capacity of the catalyst was enhanced by the good dispersion of amorphous Mn species in ZIF-8 and high specific surface area (669.7 m^2/g). This way using Mn@ZIF-8 calcined material as catalyst, molecular oxygen as green oxidant is a favorable industrial applications routine for efficient production of BOL and BAL.

Acknowledgments

The authors are grateful for the financial support of Key Research and Development Program of Hunan Province (2016NK2134), Project of Hunan Engineering Laboratory for Preparation Technology of Polyvinyl Alcohol (PVA) Fiber Material (HGY201810), Innovation Training Program for College Students of China (202110548015), Innovation Training Program for College Students of Hunan Province (S202110548055), Research Project of Huaihua University (HHUY2019-17).

References

Abdelmigeed, M.O., AlSakkari, E.G., Hefney, M.S., Ismail, F.M., Abdelghany, A., Ahmed, T.S., Ismail, I.M., 2021. Magnetized ZIF-8 impregnated with sodium hydroxide as a heterogeneous catalyst for high-quality biodiesel production. Renew Energ. 165, 405–419. https://doi.org/10.1016/j.renene.2020.11.018.

Abdollahi, B., Najafidoust, A., Asl, E.A., Sillanpaa, M., 2021. Fabrication of ZiF-8 metal organic framework (MOFs)-based CuO-ZnO photocatalyst with enhanced solar-light-driven property for degradation of organic dyes. Arab. J. Chem. 14, 103444. https://doi.org/10.1016/j.arabjc.2021.103444.

Afnan, A.H., Naim, A.S., Lina, H., Mohammad, A.H., Rula, B., Deeb, T., 2020. Synthesis of magnetic $CuFe_2O_4$ nanoparticles as green catalyst for toluene oxidation under solvent-free conditions. Arab. J. Chem. 13, 4945–4953. https://doi.org/10.1016/j.arabjc.2020.01.017.

Alabbad, S., Adil, S.F., Assal, M.E., Khan, M., Alwarthan, A., Siddiqui, M.R.H., 2014. Gold & silver nanoparticles supported on manganese oxide: Synthesis, characterization and catalytic studies for selective oxidation of benzyl alcohol. Arab. J. Chem. 7, 1192–1198. https://doi.org/10.1016/j.arabjc.2014.02.007.

Alamgholiloo, H., Rostamnia, S., Hassankhani, A., Liu, X., Eftekhari, A., Hasanzadeh, A., Zhang, K., Karimi-Maleh, H., Khaksar, S., Varma, R.S., Shokouhimehr, M., 2020. Formation and stabilization of colloidal ultra-small palladium nanoparticles on diamine-modified Cr-MIL-101: synergic boost to hydrogen production from formic acid. J. Colloid Interf. Sci. 567, 126–135. https://doi.org/10.1016/j.jcis.2020.01.087.

Alamgholiloo, H., Pesyan, N.N., Mohammadi, R., Rostamnia, S., Shokouhimehr, M., 2021. Synergistic advanced oxidation process for the fast degradation of ciprofloxacin antibiotics using a GO/CuMOF-magnetic ternary nanocomposite. J. Environ. Chem. Eng. 9, 105486. https://doi.org/10.1016/j.jece.2021.105486.

An, H., Min, K., Lee, Y., Na, R., Shim, S.E., Baeck, S.H., 2022. Sacrificial template induced Fe-, N-, and S-tridoped hollow carbon sphere as a highly efficient electrocatalyst for oxygen reduction reaction. Mol. Catal. 530, 112589. https://doi.org/10.1016/j.mcat.2022.112589.

Asadzadeh-Khaneghah, S., Habibi-Yangjeh, A., Vadivel, S., 2021. Fabrication of novel g-C_3N_4 nanosheet/carbon dots/$Ag_6Si_2O_7$ nanocomposites with high stability and enhanced visible-light photocatalytic activity. J. Taiwan Inst. Chem. Eng. 122, 320–321. https://doi.org/10.1016/j.jtice.2019.07.018.

Assal, M.E., Shaik, M.r., Kuniyil, M., Khan, M., Al-Warthan, A., Alharthi, A.I., Varala, R., Siddiqui, M.R.H., Adil, S.F., 2019. Ag_2O nanoparticles/$MnCO_3$, -MnO_2 or -Mn_2O_3/highly reduced graphene oxide composites as an efficient and recyclable oxidation catalyst. Arab. J. Chem. 12, 54–68. https://doi.org/10.1016/j.arabjc.2018.03.021.

Awadallah-F, A., Hillman, F., Al-Muhtase, S.A., Jeong, H.K., 2019. On the nanogate-opening pressures of copper-doped zeolitic imidazolate framework ZIF-8 for the adsorption of propane, propylene, isobutane, and *n*-butane. J. Mater. Sci. 54, 5513–5527. https://doi.org/10.1007/s10853-018-03249-y.

Bao, L., Yuan, X., Li, X., Yuan, X., Nuo, H., 2016. N-hydroxyphthalimide incorporated onto Cu-BTC metal organic frameworks: an novel catalyst for aerobic oxidation of toluene. Res. Chem. Intermed. 42, 5527–5539. https://doi.org/10.1007/s11164-015-2384-8.

Biswas, R., Das, S.K., Bhaduri, S.N., Bhaumik, A., Biswas, P., 2020. AgNPs immobilized over functionalized 2D hexagonal SBA-15 for catalytic C-H oxidation of hydrocarbons with molecular oxygen under solvent-free conditions, ACS Sustainable Chem. Eng. 8, 5856–5867. https://doi.org/10.1021/acssuschemeng.9b07409.

Brown, D., Hudson, R., 1951. Mechanism of hydrolysis of benzoyl chloride. Nature 167, 819. https://doi.org/10.1038/167819a0.

Chen, J., Liu, K., Jiang, M., Han, J., Liu, M., Wang, C., Li, C., 2019. Controllable preparation of porous hollow carbon sphere@ZIF-8: novel core-shell nanomaterial for Pb^{2+} adsorption. Colloid Sur. A. 568, 461–469. https://doi.org/10.1016/j.colsurfa.2019.02.044.

Chen, G., You, K., Zhao, F., Chen, Z., Luo, H., 2022. Solvent–free catalytic oxidation of toluene over heterogeneous $CeMnO_x$ composite oxides. Res. Chem. Intermed. 48, 2593–2606. https://doi.org/10.1007/s11164-022-04727-4.

Chen, G., You, K., Gong, X., Zhao, F., Chen, Z., Luo, H., 2022. Solvent-free liquid-phase selective catalytic oxidation of toluene to benzyl alcohol and benzaldehyde over CeO_2-MnO_x composite oxides. React. Chem. Eng. 7, 898–907. https://doi.org/10.1039/D1RE00488C.

Dehdashtian, S., Pourreza, N., Rostamnia, S., 2022. Electrochemical sensing of indole in plasma using Pd nanoparticles modified metal-organic framework Cr-MIL-101/ionic liquid sensor. Microchem. J. 181, 107839. https://doi.org/10.1016/j.microc.2022.107839.

Deng, Y., Dong, Y., Wang, G., Sun, K., Shi, X., Zheng, L., Li, X., Liao, S., 2017. Well-defined ZIF-derived Fe-N codoped carbon nanoframes as efficient oxygen reduction catalysts. ACS Appl. Mater. Inter. 9, 9699–9709. https://doi.org/10.1021/acsami.6b16851.

Ding, Z., Zhi, S., Wan, H., 1996. A study on wastewater minimization in indirect electrochemical synthesis of benzaldehyde. Water. Sci. Technol. 34, 113–120. https://doi.org/10.1016/S0273-1223(96)00704-4.

Du, Y., Gao, T., Ma, W., Li, H., 2018. Capacity fading of nanoporous carbon electrode derived from ZIF-8 during insertion-desertion of lithium ions. Chem. Phys. Lett. 712, 7–12. https://doi.org/10.1016/j.cplett.2018.09.051.

Fan, S., Pan, Y., Wang, H., Lu, B., Zhao, J., Cai, Q., 2017. Effect of acidic and red-ox sites over modified ZSM-5 surface on selectivity in oxidation of toluene. Mol. Catal. 442, 20–26. https://doi.org/10.1016/j.mcat.2017.09.001.

Feng, Y., Zeng, A., 2020. Selective liquid-phase oxidation of toluene with molecular oxygen catalyzed by Mn_3O_4 nanoparticles immobilized on CNTs under solvent-free conditions. Catalysts. 10, 623–635. https://doi.org/10.3390/catal10060623.

Fu, N., Ren, X., 2020. Synthesis of Double-shell hollow TiO_2@ZIF-8 nanoparticles with enhanced photocatalytic activities. Front. Chem. 8, 578847. https://doi.org/10.3389/fchem.2020.578847.

Fu, S., You, K., Chen, Z., Liu, T., Wang, Q., Zhao, F., Ai, Q., Liu, P., Luo, H., 2022. Ultrasound-assisted co-precipitation synthesis of mesoporous Co_3O_4-CeO_2 composite oxides for highly selective catalytic oxidation of cyclohexane. Front. Chem. Sci. Eng. 16, 1211–1223. https://doi.org/10.1007/s11705-022-2145-3.

Gardner, K., Mayer, J., 1995. Understanding C-H bond oxidations: H and $H^{\cdot}$ transfer in the oxidation of toluene by permanganate. Science 269, 1849–1851. https://doi.org/10.1126/science.7569922.

Guo, Y., Chen, X., Zhang, X., Pu, S., Zhang, X., Yang, C., Li, D., 2018. Comparative studies on ZIF-8 and SiO nanoparticles as carrier for immobilized β-glucosidase. Mol. Catal. 459, 1–7. https://doi.org/10.1016/j.mcat.2018.08.004.

Guo, C., Liu, Q., Wang, X., Hu, H., 2005. Selective liquid phase oxidation of toluene with air. Appl. Catal. A. 282, 55–59. https://doi.org/10.1016/j.apcata.2004.11.045.

Hao, X., Chen, C., Saito, M., Yin, D., Inoue, K., Takami, S., Adschiri, T., Ikuhara, Y., 2018. Direct imaging for single molecular chain of surfactant on CeO_2 nanocrystals. Small 14, 1093–1100. https://doi.org/10.1002/smll.201801093.

Ho, P.H., Salles, F., Renzo, F.D., Trens, P., 2020. One-pot synthesis of 5-FU@ZIF-8 and ibuprofen@ZIF-8 nanoparticles. Inorg. Chim. Acta. 500, 119229. https://doi.org/10.1016/j.ica.2019.119229.

Hu, H., Jiang, Q., Liu, Q., Song, J., Lin, W., Guo, C., 2006. Catalysis of μ-oxo-bis[porphyriniron(III)] for toluene oxidation with molecular oxygen. J. Porphyrins. Phthalocyanines. 10, 948–952. https://doi.org/10.1142/s1088424606000272.

Hu, M., Safarifard, V., Doustkhah, E., Rostamnia, S., Morsali, A., Nouruzi, N., Beheshti, S., Akhbari, K., 2018. Taking organic reactions over metal-organic frameworks as heterogeneous catalysis. Micropor. Mesopor. Mat. 256, 111–127. https://doi.org/10.1016/j.micromeso.2017.07.057.

Ilyas, M., Sadiq, M., 2009. Oxidation of toluene to benzoic acid catalyzed by platinum supported on zirconia in the liquid phase-solvent free conditions. Catal. Lett. 128, 337–342. https://doi.org/10.1007/s10562-008-9750-8.

Jian, J., Kuang, D., Wang, X., Zhou, H., Gao, H., Sun, W., Yuan, Z., Zeng, J., You, K., Luo, H., 2020. Highly dispersed Co/SBA-15 mesoporous materials as efficient and stable catalyst for partial oxidation of cyclohexane with molecular oxygen. Mater. Chem. Phys. 246, 122814. https://doi.org/10.1016/j.matchemphys.2020.122814.

Jiang, D., Mallat, T., Meier, D.M., Urakawa, A., Baiker, A., 2010. Copper metal-organic framework: Structure and activity in the allylic oxidation of cyclohexene with molecular oxygen. J. Catal. 270, 26–33. https://doi.org/10.1016/j.jcat.2009.12.002.

Jiang, F., Zhu, X., Song, F., Huang, J., Xiao, G., 2013. Au/γ-MnO_2 catalyst for solvent-free toluene oxidation with oxygen. Chin. J. Catal. 34, 1683–1689. https://doi.org/10.1016/s1872-2067(12)60633-0.

Jing, H., Wang, C., Zhang, Y., Wang, P., Li, R., 2014. Photocatalytic degradation of methylene blue in ZIF-8. RSC Adv. 4, 54454–54462. https://doi.org/10.1039/C4RA08820D.

Laribi, M., Bachari, K., Touati, M., 2016. Elaboration of nickel-impregnated over hexagonal mesoporous materials and their catalytic application. Arab. J. Chem. 9, 1388–1393. https://doi.org/10.1016/j.arabjc.2012.03.005.

Li, J., Liao, L., Jia, Y., Tian, T., Gao, S., Zhang, C., Shen, W., Wang, Z., 2022. Magnetic Fe_3O_4/ZIF-8 optimization by Box-Behnken design and its Cd(II)-adsorption properties and mechanism. Arab. J. Chem. 15, 104119. https://doi.org/10.1016/j.arabjc.2022.104119.

Li, X., Xu, J., Zhou, L., Wang, F., Gao, J., Chen, C., Ni, J., Ma, H., 2006. Liquid-phase oxidation of toluene by molecular oxygen over copper manganese oxides. Catal. Lett. 110, 149–154. https://doi.org/10.1007/s10562-006-0118-7.

Li, X., Xu, J., Zhou, L., Wang, F., Gao, J., Chen, C., Ning, J., Ma, H., 2006. Liquid-phase oxidation of toluene by molecular oxygen over copper manganese oxides. Catal. Lett. 110, 255–260. https://doi.org/10.1007/s10562-006-0118-7.

Li, X., Wang, X., Antonietti, M., 2012. Solvent-free and metal-free oxidation of toluene using O_2 and g-C_3N_4 with nanopores: Nanostructure boosts the catalytic selectivity. ACS Catal. 2, 2082–2086. https://doi.org/10.1021/cs300413x.

Liu, J., He, J., Wang, L., Li, R., Chen, P., Rao, X., Deng, L., Rong, L., Lei, J., 2016. NiO-PTA supported on ZIF-8 as a highly effective catalyst for hydrocracking of Jatropha oil. Sci. Rep-UK 6, 23667. https://doi.org/10.1038/srep23667.

Liu, P., You, K., Deng, R., Chen, Z., Jian, J., Zhao, F., Liu, P., Ai, Q., Luo, H., 2019. Hydrotalcite-derived Co-MgAlO mixed metal oxides as efficient and stable catalyst for the solvent-free selective oxidation of cyclohexane with molecular oxygen. Mol. Catal. 466, 130–137. https://doi.org/10.1016/j.mcat.2019.01.019.

Lü, B., Qi, W., Luo, M., Liu, Q., Guo, L., 2020. Fischer-tropsch synthesis: ZIF-8@ ZIF-67-derived cobalt nanoparticle-embedded nanocage catalysts. Ind. Eng. Chem. Res. 59, 12352–12359. https://doi.org/10.1021/acs.iecr.0c00971.

Mohammed, B.B., Lgaz, H., Alrashdi, A.A., Yamni, K., Tijanim, N., Dehmani, Y., Hamdani, H.E., Chung, I.M., 2021. Insights into methyl orange adsorption behavior on a cadmium zeolitic-imidazolate framework Cd-ZIF-8: A joint experimental and theoretical study. Arab. J. Chem. 14, 102897. https://doi.org/10.1016/j.arabjc.2020.11.003.

Mohtasham, H., Rostami, M., Gholipour, B., Sorouri, A.M., Ehrlich, H., Ganjali, M.R., Rostamnia, S., Rahimi-Nasrabadi, M., Salimi, A., Luque, R., 2022. Nano-architecture of MOF (ZIF-67)-based Co_3O_4 NPs@N-doped porous carbon polyhedral nanocomposites for oxidative degradation of antibiotic sulfamethoxazole from wastewater. Chemosphere. 310, 136625. https://doi.org/10.1016/j.chemosphere.2022.136625.

Movahed, S.K., Piraman, Z., Dabiri, M., 2018. A nitrogen-doped porous carbon derived from copper phthalocyanines on/in ZIF-8 as an efficient photocatalyst for the degradation of dyes and the Csingle bondH activation of formamides. J. Photoch. Photobio. A. 351, 208–224. https://doi.org/10.1016/j.jphotochem.2017.10.026.

Musić, S., Ristić, M., Popović, S., 2009. Synthesis and microstructure of porous Mn-oxides. J. Mol. Struct. 924-926, 243–247. https://doi.org/10.1016/j.molstruc.2008.10.005.

Nagarjun, N., Dhakshinamoorthy, A., 2019. A Cu-Doped ZIF-8 metal organic framework as a heterogeneous solid catalyst for aerobic oxidation of benzylic hydrocarbons. New. J. Chem. 43, 18702. https://doi.org/10.1039/c9nj03698a.

Ni, W., You, K., Yi, L., Zhao, F., Ai, Q., Liu, P., Luo, H., 2021. Highly selective preparation of cyclohexanone oxime from liquid-phase catalytic oxidation of cyclohexylamine with molecular oxygen over glucose-modified TiO_2 under solvent-free conditions. Ind. Eng. Chem. Res. 60, 3907–3913. https://doi.org/10.1021/acs.iecr.0c05755.

Partenheimer, W., 2003. The effect of zirconium in metal/bromide catalysts during the autoxidation of *p*-xylene: Part i. Activation and changes in benzaldehyde intermediate formation. J. Mol. Catal. A: Chem. 206, 105–119. https://doi.org/10.1016/S1381-1169(03)00407-2.

Pliekhov, O., Pliekhov, O., LavrenčičŠtangar, U., Logar, N.Z., 2018. The Co-MOF-74 modified with N, N′-dihydroxypyromellitimide for selective, solvent free aerobic oxidation of toluene. Catal. Commun. 110, 88–92. https://doi.org/10.1016/j.catcom.2018.03.021.

Ran, J., Chen, H., Bi, S., Guo, Q., Deng, Z., Cai, G., Cheng, D., Tang, X., Wang, X., 2020. One-step in-situ growth of zeolitic imidazole frameworks-8 on cotton fabrics for photocatalysis and antimicrobial activity. Cellulose 27, 10447–10459. https://doi.org/10.1007/s10570-020-03483-1.

Rezaei, M., Chermahini, A.N., Dabbagh, H.A., 2017. Selective oxidation of toluene to benzaldehyde by H_2O_2 with mesoporous silica KIT-6 supported $VOHPO_{40}5H_2O$ catalyst. J. Environ Chem. Eng. 5, 3529–3539. https://doi.org/10.1016/j.jece.2017.07.019.

Somma, I.D., Russo, D., Andreozzi, R., Marotta, R., Guido, S., 2017. Kinetic modelling of benzyl alcohol selective oxidation in aqueous mixtures of nitric and sulfuric acids. Chem. Eng. J. 308, 738–744. https://doi.org/10.1016/j.cej.2016.09.113.

Son, S., Lim, D., Nam, D., Kim, J., Shim, S.E., Baeck, S.H., 2019. N, S-doped nanocarbon derived from ZIF-8 as a highly efficient and durable electro-catalyst for oxygen reduction reaction. J. Solid State. Chem. 274, 237–242. https://doi.org/10.1016/j.jssc.2019.03.036.

Taghavi, R., Rostamnia, S., Farajzadeh, M., Karimi-Maleh, H., Wang, J., Kim, D., Jang, H., Luque, R., Varma, R., Shokouhimehr, M., 2022. Magnetite metal-organic frameworks: applications in environmental remediation of heavy metals, organic contaminants, and other pollutants. Inorg. Chem. 61, 15747–15783. https://doi.org/10.1021/acs.inorgchem.2c01939.

Tan, S., Xia, T., Shi, Y., Pfaendtner, J., Zhao, S., He, Y., 2017. Enhancing the oxidation of toluene with external electric fields: a reactive molecular dynamics study. Sci. Rep. 7, 1–11. https://doi.org/10.1038/s41598-017-01945-4.

Wang, Z., Lai, C., Qin, L., Fu, Y., He, J., Huang, D., Li, B., Zhang, M., Liu, S., Li, L., Zhang, W., Yi, H., Liu, X., Zhou, X., 2020. ZIF-8-modified $MnFe_2O_4$ with high crystallinity and superior photo-Fenton catalytic activity by Zn-O-Fe structure for TC degradation. Chem. Eng. J. 392, 124851. https://doi.org/10.1016/j.cej.2020.124851.

Wang, B., Mao, W., Ma, H., 2009a. A mild simple method for liquid-phase selective catalytic oxidation of toluene with ozone over CeO_2 promoted sulfated TiO_2. Ind. Eng. Chem. Res. 48, 440–445. https://doi.org/10.1021/ie800725h.

Wang, X., Wu, J., Zhao, M., Lv, Y., Li, G., Hu, C., 2009b. Partial oxidation of toluene in CH_3COOH by H_2O_2 in the presence of VO $(acac)_2$ catalyst. J. Phys. Chem. C 113, 14270–14278. https://doi.org/10.1021/jp9028062.

Wen, J., You, K., Chen, M., Jian, J., Zhao, F., Liu, P., Ai, Q., Luo, H., 2021. Mesoporous silicon sulfonic acid as a highly efficient and stable catalyst for the selective hydroamination of cyclohexene with cyclohexylamine to dicyclohexylamine in the vapor phase. Front. Chem. Sci. Eng. 15, 654–665. https://doi.org/10.1007/s11705-020-1973-2.

Xiang, B., Fu, L., Li, Y., Liu, Y., 2019. Two synthesis methods for Fe (III)@MOF-5-derived porous carbon composites for enhanced phenol hydroxylation. ChemistrySelect. 12, 13638–13645. https://doi.org/10.1002/slct.201902941.

Xu, J., Shi, G., Liang, Y., Lu, Q., Ji, L., 2021. Selective aerobic oxidation of toluene to benzaldehyde catalyzed by covalently anchored N-hydroxyphthalimide and cobaltous ions. Mol. Catal. 503, 111440. https://doi.org/10.1016/j.mcat.2021.111440.

Yang, X., Wen, Z., Wu, Z., Luo, X., 2018. Synthesis of ZnO/ZIF-8 hybrid photocatalysts derived from ZIF-8 with enhanced photocatalytic activity. Inorg. Chem. Front. 5, 687–693. https://doi.org/10.1039/C7QI00752C.

Yang, X., Chen, W., Bian, H., Sun, T., Zhang, Z., Zhang, W., Du, Y., Li, Y., Chen, X., Wang, F., 2018. Synthesis of mesoporous ZIF-8 nanoribbons and their conversion into carbon nanoribbons for high-performance supercapacitors. Chem. Eur. J. 24, 11185–11192. https://doi.org/10.1002/chem.201801869.

Zhang, Y., Li, C., He, X., 2008. Simulation and optimization in the process of toluene liquid-phase catalytic oxidation. Chin. J. Chem. Eng. 16, 36–38. https://doi.org/10.1016/s1004-9541(08)60032-4.

Zhang, C., Liao, P., Wang, H., Sun, J., Gao, P., 2018. Preparation of novel bimetallic CuZn-BTC coordination polymer nanorod for methanol synthesis from CO_2 hydrogenation. Mater. Chem. Phys. 215, 11–20. https://doi.org/10.1016/j.matchemphys.2018.05.028.

Zhang, X., Qi, M., Zhang, G., Lin, T., Gong, T., 2011. Solvent-free liquid phase oxidation of benzyl alcohol to benzaldehyde over superfine $MgAl_2O_4$ supported Co-based catalysts: effects of support $MgAl_2O_4$. Adv. Mater. Res. 233–235, 1100–1107. https://doi.org/10.4028/www.scientific.net/AMR.233-235.1100.

Zhang, S., Xu, Y., Zhao, D., Chen, W., Li, H., Hou, C., 2020. Preparation of magnetic $CuFe_2O_4$@Ag@ZIF-8 nanocomposites with highly catalytic activity based on cellulose nanocrystals. Molecules 25, 124–139. https://doi.org/10.3390/molecules25010124.

Zhao, J., Han, W., Zhang, J., Tang, Z., 2020. In situ growth of Co_3O_4 nano-dodecahedeons on In_2O_3 hexagonal prisms for toluene catalytic combustion. Arab. J. Chem. 13, 4857–4867. https://doi.org/10.1016/j.arabjc.2020.01.014.

Zhao, Y., Liu, Y., Cao, J., Wang, H., Shao, M., Huang, H., Liu, Y., Kang, Z., 2020. Efficient production of H_2O_2 via two-channel pathway over ZIF-8/C_3N_4 composite photocatalyst without any sacrificial agent. Appl. Catal. B: Environ. 278, 119289. https://doi.org/10.1016/j.apcatb.2020.119289.

Zheng, H., Wu, D., Wang, Y., Liu, X., Gao, P., Liu, W., Wen, J., Rebrov, E.V., 2020. One-step synthesis of ZIF-8/ZnO composites based on coordination defect strategy and its derivatives for photocatalysis. J. Alloys Compd. 838, 155219. https://doi.org/10.1016/j.jallcom.2020.155219.

Zhu, Y., Wang, H., Wang, B., Liu, X., Wu, H., Licht, S., 2016. Solar thermoelectric field plus photocatalysis for efficient organic synthesis exemplified by toluene to benzoic acid. Appl. Catal. B: Environ. 193, 151–159. https://doi.org/10.1016/j.apcatb.2016.04.024.